

Jets and Tori in Proto-Planetary Nebulae

P. J. Huggins

Physics Department, New York University, 4 Washington Place, New York, NY 10012

patrick.huggins@nyu.edu

ABSTRACT

We investigate the time sequence for the appearance of jets and molecular tori in the transition of stars from the Asymptotic Giant Branch to the planetary nebula phase. Jets and tori are prominent features of this evolution, but their origins are uncertain. Using optical and millimeter line kinematics, we determine the ejection history in a sample of well-observed cases. We find that jets and tori develop nearly simultaneously. We also find evidence that jets typically appear slightly later than tori, with a lag time of a few hundred years. These characteristics provide strong evidence that jets and tori are physically related, and they set new constraints on theories of jet formation. The ejection of a discrete torus followed by jets on a short time scale favors the class of models in which a companion interacts with the central star. Models with long time scales, or with jets followed by a torus, are ruled out.

Subject headings: circumstellar matter — planetary nebulae: general — stars: AGB and post-AGB — stars: mass loss

1. Introduction

Planetary nebulae (PNe) are observed to exhibit remarkably complex morphologies that are not well understood (e.g., Balick & Frank 2002; Meixner et al. 2004). Point symmetry is the most striking characteristic of the nebulae and is known to be produced by the action of high velocity jets which emanate from the central star system and interact with the circumstellar gas. The jets are typically bipolar, but may show multiple components or changes in direction. They are widely seen in young PNe and proto-PNe (e.g., Sahai & Trauger 1998) and, in a few cases, in the final stages of the Asymptotic Giant Branch (AGB) (e.g., Imai et al. 2002). The origin of the jets is, however, uncertain.

Four different types of scenario have been proposed for the formation of the jets: a magnetic wind from single stars (García-Segura et al. 2005); an accretion disk around a

binary companion, fed by the mass-loss of the primary (Morris 1987; Soker & Rappaport 2000); a magnetic (possibly explosive) wind from the primary, spun up by a companion (e.g., Nordhaus & Blackman 2006; Matt et al. 2006), and an accretion disk around the core of the primary, formed by the overflow or break-up of a binary companion during or after a common envelope phase (Soker & Livio 1994; Soker 1996; Reyes-Ruiz & López 1999; Nordhaus & Blackman 2006). In all these cases the region of jet launching is too small to be resolved by current observations. Our constraints on the process of jet formation are, therefore, necessarily indirect, based on their large scale properties and our understanding of the environment in which they form.

A second, extremely common characteristic of PNe and proto-PNe is a region of equatorially enhanced mass loss. This often forms a relatively well defined structure, variously described as a ring, or torus. The mass of this component may be large, $\gtrsim 0.1 M_{\odot}$ with corresponding mass loss rates $\gtrsim 10^{-4} M_{\odot} \text{ yr}^{-1}$ (e.g., Huggins et al. 2004), $\gtrsim 1$ –2 orders of magnitude larger than typical mass loss rates on the upper AGB. The origin of this enhanced mass loss is not known for certain, but it terminates the evolution of the star on the AGB and occurs in the same transition phase as the first appearance of prominent jets.

In this paper we explore possible relations between the ejection of the tori and the development of jets. We determine the timing of their appearance as accurately as possible using the kinematic structure of a sample of well-observed transition objects, and use the results to evaluate different jet formation scenarios.

2. Observations

In order to investigate the time sequence for the appearance of jets and tori we consider transition objects whose dimensions, kinematics, and orientation are sufficiently well characterized by observations that we can estimate when these features formed. The sample is listed in Table 1. It includes late AGB stars, proto-PNe, and young PNe, although the status of M 2-9, which is usually included among young PNe is uncertain; it may be a symbiotic system, e.g., Corradi (2004). For convenience, we shall call the objects proto-PNe as a group. Column (2) of the table gives the adopted distances for later use.

The objects in Table 1 were selected on the basis of the following criteria: they show well defined jets and tori; the kinematic structure of the tori has been observed in millimeter CO emission at high angular resolution; and the kinematics of the jets have been observed in molecular lines, or at optical wavelengths. In fact, the sample includes most of the transition objects that have so far been mapped at high resolution in CO; we have omitted only a few

cases in which the jets or equatorial regions are complex, e.g., AFGL 2688 (Cox et al. 2000), or the geometry is poorly determined. The emphasis here on molecular line observations of the tori is important for providing robust reconstructions of the ejection history. There are, of course, many optical observations of the equatorial regions of fully formed PNe, but in these cases the dynamical effects of pressure in the ionized gas make reconstruction of the ejection history subject to large systematic uncertainty.

Table 1 summarizes the data on the sample objects. Columns (3)–(4) give estimates for the radii and expansion velocities of the equatorial tori (r_t and v_t) for each object, and columns (6)–(7) give the radial extents and velocities for the jets (r_j and v_j). The observations on which these values are based are reported in the references in the table. The adopted values are taken from spatio-kinematic models or data summaries by the authors cited, or are based on new estimates made from maps given in the papers. The observations are corrected for projection using data on the inclination angles (which we take to be the angle between the axis of the torus or the jets, to the line of sight) given in the appendix. The values of r_t and r_j are calculated using the distances given in column (2) of Table 1.

The data for the tori are based on interferometric CO observations. The values of r_t refer to characteristic radii of the tori. In cases where the inner hole is resolved by the observations, r_t is the radius of peak CO emission or the mean of inner and outer radii from model fits by the authors. If the inner hole is marginally resolved or not resolved, r_t gives the radius modeled by the authors, or the half-intensity radius estimated from the CO emission maps. The data for the jets are based on molecular line or optical observations. The values of r_j and v_j refer to the prominent jet heads farthest from the center of the system. These data are typically averages for oppositely directed jets, but only one is used if the data for it are superior.

The data on the radial extents and velocities of the jets and tori are used to determine the expansion times given by $t_j = r_j/v_j$ and $t_t = r_t/v_t$. These are listed in columns (5) and (8) of Table 1. For three objects (He 3-1475, M 2-9, and KjPn 8), we have preferred to use expansion times for the jets determined from optical proper motions, because they are generally more accurate and are independent of the inclination angle. In these cases $t_j = \phi/\dot{\phi}$ where ϕ is the angular distance of the jet head from the central star and $\dot{\phi}$ is its time derivative.

In summary, the expansion times of the tori are all determined from molecular line observations, while the expansions times of the jets are from molecular line kinematics, optical line kinematics, or optical proper motions. In two cases, M 1-16 and He 3-1475, there are measurements of additional jet heads closer to the central star system. Information on these and further details of the observations are given in the appendix.

3. Timing

3.1. Near Simultaneity

We use the expansion times of the jets and tori as estimates for the time since they were ejected from the central star systems. The large masses and low expansion velocities of the dense molecular tori mean that their expansion times (t_t) provide excellent estimates for their travel times. For the jets, there is a good deal of observational evidence from detailed studies of individual objects for approximately Hubble-type outflows that also suggest constant velocity, ballistic motions (e.g., Alcolea et al. 2001; Corradi 2004; Ueta et al. 2006). We assume that this applies to the jet heads considered here. We discuss this assumption further in §3.2.

Fig. 1 compares the expansion times of the jets with the expansion times of the tori. The squares denote cases where the torus is resolved, and the diamonds denote cases where it is not well resolved. The solid line shows the relation $t_j = t_t$.

One major uncertainty that affects the location of the data points in Fig. 1 is caused by uncertain distances to the nebulae. Apart from the exceptions noted below, this affects both t_j and t_t in the same way: it moves the plotted points parallel to the line $t_j = t_t$ in the figure and does not appreciably affect our discussion.

A second important effect that affects the location of the data points in Fig. 1 is uncertainty in the inclination angles of the jets and tori. The adopted values and estimates of the uncertainties are given in the appendix. In most cases the values of t_t and t_j vary with inclination as $\sin \theta$ and $\cot \theta$, respectively, and the error bars shown in Fig. 1 represent the uncertainty due to the inclination angle. For the three objects whose jet expansion times are determined from proper motions, t_j is independent of the inclination and the distance, and the error bars in the figure reflect the formal errors from the proper motions. For these objects, the distance does contribute to the uncertainty in t_t , but in all cases it is well determined (to within $\sim \pm 15\%$, see references in Table 1), and for simplicity this additional contribution is omitted in the figure.

A third effect, which is important for He 3-1475 and AGFL 618, arises because their equatorial regions are only marginally resolved by the observations so the dimensions of the tori are not well determined. In both cases the values for the torus parameters are taken from models of the CO emission (see appendix). The errors are difficult to quantify but are probably within a nominal overall factor of two in t_t , and these are shown as gray error bars in the figure.

The expansion times of the jets and tori shown in Fig. 1 span a large range, from

~ 100 yr to several 1000 yr. In spite of the heterogeneity of the data and the uncertainties in individual cases, the figure shows that the ages of the jets and the ages of the tori are well correlated, and that the data points lie not far from the line $t_j = t_t$. The implication is that the torus and jets in each object were ejected nearly simultaneously.

It is also of interest to note that the ejection ages are roughly ordered according to the degree of evolution indicated by the spectral type of the star and/or the development of the nebula: i.e., from youngest to oldest corresponds to AGB stars, through proto-PNe (typically B-type spectra), to true PNe. This is consistent with all ejections (except perhaps M2-9 whose status is uncertain, see §2) happening in the final stages of the AGB phase, or shortly thereafter.

3.2. Jet-Lag

The jets and tori have similar ages, but the data points in Fig. 1 lie systematically below the line $t_j = t_t$. The effect appears more pronounced for the younger systems in the log-log plot, but it is also present for the older systems as well. The data in a few cases are consistent with $t_j = t_t$ within the uncertainties, but for all objects our best estimates of the time difference $\Delta t = t_t - t_j$ (column 9 in Table 1) are positive. This ordering has previously been noted in individual cases (e.g., Forveille et al. 1998; Huggins et al. 2000; Sánchez Contreras et al. 2004), but the result for the ensemble as a whole makes it much more concrete, especially in view of the fact that t_j refers to the heads of the jets, and t_t refers to the mean radius of the tori (or some similar measure) in most cases. In fact, given the diversity of the data used to compile the figure, the uniformity of the effect is striking.

There are two likely explanations of the observed effect that need to be considered, and we discuss each in turn. The first is that the values of t_j and t_t are good approximations to the actual travel times of the jets and tori (as previously assumed), but the jets and tori are not exactly simultaneous. The observed effect is produced if the jets are slightly younger than the tori, i.e., there is a small but systematic delay in the launching of the jets relative to the tori. If so, this delay, or jet-lag, is given by the value of Δt . It might correspond, for example, to a power-up time for the jets, or an accretion time scale (§4.2.2). Inspection of Table 1 (column 9) shows that the largest value of Δt is for the oldest system (KjPn 8), but the others are comparable, within the large uncertainties. The median jet-lag is 300 yr.

The second explanation to consider is that the jets and tori are ejected simultaneously, but the expansion times differ from the actual travel times. The expansion times of the massive molecular tori are almost certainly good approximations to the travel times for

reasons given earlier. In the event that they are formed deep within the star, they could be decelerated by overlying layers, but this is unlikely to affect the timing over the large distances and long time intervals accessible to the observations. We therefore confine our attention to the jets. These move through the circumstellar environment at high velocity, and from a theoretical point of view their kinematic behavior is uncertain, so we consider various possibilities in turn.

If the ejection of a jet is short-lived, the jet head may act as a bullet, in which case it would travel at a constant velocity, or decelerate to the extent that it interacts with ambient circumstellar gas. The deceleration of He 3-1475 has been considered by Riera et al. (2003) and is estimated to be relatively small, although the theory of bullet interactions with ambient gas is not fully developed. More generally, if the head decelerates, it can be seen by writing the actual travel time as $t = \int dr/v(r)$ that the value of t_j given by the current (observed) value of r_j/v_j (or the equivalent proper motion $\phi/\dot{\phi}$) overestimates the travel time. Therefore, if the ejections of the jets and tori were simultaneous, the apparent ages of the jets would be older than the tori, an effect opposite to that seen in Fig. 1. We conclude that deceleration does not dominate the observations, and if it were to play any quantitative role, the true jet-lag would be larger than that tabulated in Table 1.

A different situation occurs if the jet is continuous over an extended interval of time. To illustrate this case, we consider a jet driven through the circumstellar gas by a radial, momentum-conserving, fast outflow, with a narrow, fixed, opening angle. For an envelope with a density that varies as r^{-2} , which corresponds to a constant mass loss rate, the velocity of the jet head is a constant to first order (Lee et al. 2001). However, according to the simulations of Lee & Sahai (2003), the effects of the motion of material along the sides of the jets may lead to a small acceleration. The velocity of the jet head may then be written as $v = u_j(1 + \alpha t)$, where u_j is the initial velocity and α is a parameter with a typical value $\sim 10^{-3} \text{ yr}^{-1}$ for the simulations they present. If the jets and tori were ejected simultaneously, we can identify t with t_t and would expect the apparent ages of the jets to be smaller than the ages of the tori by Δt given by:

$$\frac{\Delta t}{t} = \frac{\alpha t}{2(1 + \alpha t)}. \quad (1)$$

This expression has values of $\alpha t/2 \sim 0, 0.25,$ and $0.5,$ for $\alpha t \ll 1, \alpha t = 1,$ and $\alpha t \gg 1,$ respectively. For an ensemble of objects, we then expect $\Delta t/t$ to range from near zero for young systems, up to 0.5 for very old systems. The observed values are listed in column (10) of Table 1. They show the opposite behavior, with the largest values for the youngest systems. It is not possible to rule out acceleration in any individual case, but there is no strong evidence for it from the ensemble of data. In view of this, and the extensive

empirical evidence for approximately Hubble-like jet flows cited earlier, we conclude that jet acceleration is probably not the primary effect, and that the jet-lag sequence is the preferred one.

On the basis that the expansion times are reasonable approximations of the travel times, we can reconstruct the time evolution of the torus-jet sequence. The time line for each object is shown in Fig. 2. The filled symbols denote the values of t_t already discussed, and represent the average or characteristic expansion times of the tori. The horizontal lines represent the time interval over which the tori are ejected. These are based on the radial extents of the tori (e.g., the half intensity widths or model fits to the radial extent), and assuming the ejection takes place at the mean expansion velocity for each object listed in the Table 1. If the tori are ejected with a significant dispersion in velocity, the time lines overestimate the width of the corresponding ejection interval. M 1-92 may be an extreme case with a velocity gradient that suggests it was ejected in a short time (Alcolea et al. 2007, see also Appendix A2). The information on the partially resolved tori (AFGL 618 and He3-1475) is incomplete. The triangles on each line in Fig. 2 denote the times at which the jets are ejected, and are subject to the uncertainties in timing discussed above. For two objects, M 1-16 and He 3-1475, the timing of later jets (see appendix) is also shown, to illustrate the overall sequence.

The ejection sequences for all the objects shown in Fig. 2 are qualitatively similar. There is a rapid build-up of the torus and then the jets are launched, and may reoccur. As discussed above, our best estimates suggest a finite lag time for the jets, with a median of 300 yr. If this is measured with respect to the onset of the torus ejection, it is probably somewhat longer. The interval between the jets in the objects with a sequence of jets is comparable to the jet-lag time.

4. Discussion

4.1. Jets and Tori

The ejection of jets and tori are among the most important events in the transition of stars from the AGB to the PN phase. Our finding that they occur close together in time provides strong evidence that they are physically related, either causally, or by some underlying process or event linking the two.

Our additional finding that jets and tori probably occur in a particular sequence, underscores their connection. These results, together with the time-scale for the torus ejection and the time scale for the torus-jet sequence, provide basic constraints on formation scenarios.

Despite their connections, it is important to emphasize that the actual ejections of jets and tori are different in character. The jets involve high velocity, axial outflows, while the tori involve low velocity equatorial outflows. The difference in the velocities is highlighted by the data listed in Table 1. The median velocity of the jets is 160 km s^{-1} and the median velocity of the tori is 10 km s^{-1} . It is noteworthy that the latter is comparable to, but below the typical wind velocity on the upper AGB: the median envelope velocities for bright carbon stars, infrared carbon stars, and OH/IR stars, are 11.4 km s^{-1} , 17.8 km s^{-1} , and 13.6 km s^{-1} , respectively (Olofsson 2003). In addition, in the individual cases M 1-16 (Huggins et al. 2000) and AFGL 618 (Sánchez Contreras et al. 2004), the tori have lower expansion velocities than the extended AGB envelopes. Thus the torus ejection, which may also involve a very high mass-loss rate (§1), is likely to be a different process from, or at least a modification of, the regular AGB mass loss.

4.2. Formation Scenarios

The linking of jets and tori, and their related time scales, considerably extend the range of constraints we have on jet formation. In the following, we comment on how these considerations affect our evaluation of specific scenarios that have been proposed. Table 2 is used to help keep track of the different possibilities.

4.2.1. *Magnetic Winds from Single Stars*

One scenario for jet formation proposed by García-Segura and co-workers is a collimated wind from single stars in the proto-PN phase. Their models (e.g., García-Segura et al. 2005) do not appear to naturally give rise to the ejection of a torus close in time with the jets. The equatorial density enhancements that are featured in some of their simulations are input separately, and do not appear to constitute a discrete ejection. In view of the close connection between jets and tori presented in this paper, the single star models do not currently give a good description of the observations.

4.2.2. *Companion Accretion Disks*

A second class of scenarios for jet formation occurs in binary systems where part of the matter lost in the wind of the evolving AGB star (the primary) is captured by a binary companion (the secondary) and forms a disk (Morris 1987; Soker & Rappaport 2000). The

disk in turn forms jets. The jet launching mechanism is not known for certain, but is probably similar to that in young stellar objects (e.g., Frank & Blackman 2004).

There is growing evidence for binary interactions in AGB stars with high mass loss rates (e.g., Mauron & Huggins 2006), and the binary accretion disk scenario is consistent with our findings on several points. (1) The presence of a close binary provides a mechanism to enhance the mass loss of the primary, and to preferentially confine the mass loss to the orbital plane. (2) If a discrete torus forms, the increase in mass loss produces an increase in the accretion rate of the disk; assuming that jets are enhanced or perhaps triggered by the increased accretion, this model provides the basis of a causal link between tori and jets. (3) This causal relationship also has the potential to account for the delay in launching the jets.

The delay due to the travel time of material between the primary and the secondary is expected to be small under most circumstances, e.g., $\Delta t = 5$ yr for a separation of 10 AU and a gas velocity of 10 km s^{-1} . However, a significant delay could arise because it takes a finite time for matter accreted by a disk to spiral into the inner regions where the jets are presumably launched. In the present scenario, the increased accretion rate of the disk will occur during the build-up of the torus, so that the jets will be delayed by a time comparable to the accretion time of the disk. This is given by the expression $t_\nu = R^2/\nu$, where R is the radius of the disk and ν is the viscosity. In the α -prescription (Shakura & Sunyaev 1973), this can be parameterized as:

$$t_\nu = 160 \text{ yr} \left(\frac{\alpha}{0.1} \right)^{-1} \left(\frac{R}{1 \text{ AU}} \right)^{3/2} \left(\frac{M_2}{1 M_\odot} \right)^{-1/2} \left(\frac{H/R}{0.1} \right)^{-2}, \quad (2)$$

where α is the usual viscosity parameter, M_2 is the mass of the companion, and H is the scale height of the disk.

The sizes of the disks are unknown, but simulations of accretion by relatively close companions (Theuns & Jorissen 1993; Mastrodemos & Morris 1999) and tidal truncation (Pastetter & Ritter 1989) suggest disks with radii ~ 1 AU may be formed. For disks of this size and reasonable values for the companion mass and disk thickness, it can be seen that if α is as low 10^{-3} – 10^{-4} as found by Bell & Lin (1994) to reproduce the flaring time of FU Ori stars, the accretion times would be $\gtrsim 10^4$ yr. This kind of time scale is completely ruled out by the short jet-lags observed. For a typical jet-lag of ~ 300 yr, a disk of radius 1 AU requires $\alpha \gtrsim 0.05$. Thus, if this model proves relevant, the jet-lag has the potential to probe properties of the disks that are currently unobservable in any other way.

The points outlined above are consistent with the binary accretion disk model. In addition, if M 2-9 proves to be a symbiotic system with a detached companion (see §2), it adds support to this interpretation. There is, however, one aspect of the observations that is

not naturally explained by this scenario, and that is the ejection of a torus. Enhanced mass-loss is certainly a feature expected in close binary systems, but the formation mechanism of a discrete torus is unclear.

In their binary model for PNe with narrow waists, Soker & Rappaport (2000) argue that the tori are formed by the effects of a collimated fast wind (i.e., the jets) from the companion, by concentrating the AGB wind toward the equatorial plane. If the fast wind extends over a wide angle in latitude and forms a hot bubble, it may contribute to the equatorial concentration, but the simulations of García-Arredondo & Frank (2004) with more directed jets show mainly local enhancements around the flow cavities and no clear build up of a large scale torus. In any event the relatively sudden appearance of low velocity tori with large masses (and large mass loss rates) cannot be explained by simply compressing the gas in latitude. A trigger or event to produce the tori is much more likely. One possibility is magnetic expulsion along the lines discussed in the next section, powered by spin-up of the envelope, and triggered at a point when the overlying mass of the AGB envelope is reduced to a critical level. This and other ways to generate a torus within this scenario warrant further attention.

A variant of the binary accretion disk scenario is one in which a disk first forms around the companion and blows jets (e.g., as a result of wind accretion or Roche lobe overflow of the primary), and then enters the primary in a common envelope and ejects a torus (see next section). This sequence of jets followed by a torus is ruled out by the observations.

4.2.3. *Magnetic Effects in Common Envelopes*

A range of scenarios for jet formation occurs where there is direct interaction between a close binary companion and the AGB star in a common envelope phase (Iben & Livio 1993). In this phase, the companion is engulfed by the AGB star: it may spiral in toward the center on a rapid time scale $\lesssim 10$ yr, and if the mass of the companion is above $\sim 0.1 M_{\odot}$, it can deposit enough energy to eject a significant portion of the AGB envelope (e.g., Soker & Livio 1994; Nordhaus & Blackman 2006). Simulations show that the envelope is ejected on a short time scale (~ 1 yr), mainly in the equatorial plane of the system (Sandquist et al. 1998). The ejection, therefore, provides a natural mechanism for the formation of an expanding torus.

During the interaction, the envelope may be spun up by the secondary, and this can enhance the magnetic field by dynamo action to produce a jet, with a short lifetime $\lesssim 100$ yr (Nordhaus & Blackman 2006). If both spin-up and ejection occur during the common

envelope phase, this would generate jets and a torus close in time as observed. It remains to be seen from detailed simulations whether the jet-lag sequence is a natural feature of this scenario.

A related scenario discussed by Matt et al. (2006) is one in which rotational shear between the core and envelope builds up the magnetic field until it explodes in both the polar and equatorial directions. This case is attractive because the jets and torus are likely to form close in time, as observed, and the magnetic field in the torus may have observable characteristics (Huggins & Manley 2005; Sabin et al. 2007). Again, it remains to be seen from detailed simulations whether the jet-lag sequence is a natural feature of this scenario.

In either the hydrodynamic or the magnetic expulsion of the equatorial gas, a very important constraint provided by the ensemble of observations in Table 1 is the low velocity of the tori (Table 1). The ejection of matter from the deep potential well of a close binary or in a magnetic explosion likely leads to a range of ejection velocities and this point needs to be evaluated in realistic simulations. If the simulations are unable to produce coherent low velocity tori, these formation mechanisms could be ruled out.

Several other considerations bear on this class of scenarios. In the case of V Hya (Table 1), Barnbaum et al. (1995) have found that the photospheric lines are broadened, and interpret this as evidence that the star is currently in the common envelope phase. If this is so, the radially extended torus (Hirano et al. 2004) implies an extended interval of equatorial mass-loss of ~ 1500 yr as shown in Fig. 2. This is much longer than the ejection times found in simulations of common envelope ejection noted above. On the other hand, Knapp et al. (1999) find evidence for a 17 yr period in V Hya, which may indicate a detached binary system.

In the case of M 1-92 (Table 1), Alcolea et al. (2007) interpret their observations to indicate that the jets and torus are exactly simultaneous, and therefore support the magnetic explosion model. For the best available estimate of the inclination angle of the system that we adopt (see appendix), the jets are marginally younger than the torus, as in all the other objects, so there is no compelling reason that they must be simultaneous. It is also true that the magnetic expulsion models are at very early stages of exploration; they may not in fact give rise to exactly simultaneous polar and equatorial ejections and may be consistent with the jet-lag picture.

4.2.4. *Primary Accretion Disks*

A further class of scenarios that may produce jets involves a binary companion that forms an accretion disk around the primary during or after the common envelope phase.

If the companion is of low mass (brown dwarf or planet), it enters the AGB star and spirals in toward the core, where it is gravitationally shredded to form a disk that may blow jets through the envelope (Soker 1996; Reyes-Ruiz & López 1999; Nordhaus & Blackman 2006). A very low mass secondary has insufficient energy to eject much of the AGB envelope during the spiral-in process, so it does not naturally lead to the formation of a massive torus. However, the primary may go on to later eject the envelope, possibly with an equatorial enhancement. In this scenario, there is no particular co-ordination of jets and torus, and it yields a sequence of jets followed by a torus, which is opposite to that observed in all the objects discussed here. This scenario can be rejected.

In a variant of this scenario (Nordhaus & Blackman 2006), the mass of the secondary may be enough to eject part of the AGB envelope in a torus before the companion is shredded to form a disk. This leads to a torus-jet sequence, as observed. The time sequence is likely to be short because the spiral-in and break-up times are rapid, but a viscous jet-lag of the form given by equation (2) may be relevant, if the viscosity parameter is low enough to compensate for a small disk radius.

An alternative scenario with an accretion disk around the primary occurs when the secondary is a main sequence star of mass $\gtrsim 0.1 M_{\odot}$. In this case, the envelope of the AGB star is ejected in the common envelope phase as a torus; the spiral-in process of the secondary comes to halt, but it may subsequently undergo Roche lobe overflow to form a disk around the primary (Soker & Livio 1994). This produces a clear torus-jet sequence as observed. However, there are two problems with this scenario. First, the timescale between the torus ejection and the disk-jet formation is governed by the thermal response time of the secondary, which is 10^3 – 10^4 yr (Soker & Livio 1994). This is somewhat too long compared with the typical jet-lag sequence that we find from the observations. The second problem is that the jets in this scenario are produced after the common envelope phase. It seems unlikely that the coolest objects that we consider (which have already formed jets) are post common-envelope; this may also apply to all the objects in the sample given the ages of their jets and their likely evolution times across the H-R diagram. Except for the ejection plus break-up case noted above, these primary disk scenarios are not well matched to the observations.

It is interesting to note that Mitchell et al. (2006) have recently reported on the kinematics of the PN Abell 63, which has a close binary central star and must have gone through

a common envelope phase. Mitchell et al. (2006) find that the lobes (jets) in Abell 63 are older than the nebular rim which forms the inner edge of a cylindrical torus. They conclude that this is consistent with jets formed after a common envelope (from a disk around the primary core) but before formation of the main nebula. As remarked above, the sequence of jets followed by a torus is the opposite of all the cases discussed in this paper. It could be that Abell 63 is different. On the other hand, the jets are very old (13,000 yr), so it is unclear if simple kinematics can be used to infer such long travel times. In addition, the age of the rim is determined from observations of ionized gas whose dynamical evolution during the formation of the nebula is uncertain. In view of these caveats, the conclusions of Mitchell et al. (2006) on the jet sequence in Abell 63 need to be viewed with some caution.

4.2.5. *Summary Evaluation*

From the above discussion, it can be seen that there are quite a number of scenarios that might potentially produce jets in proto-PNe, and it may be that more than one of them actually occurs. However, the properties of the objects discussed in this paper, with well defined jets and molecular tori, are sufficiently uniform that a common mechanism seems most reasonable.

On this basis, our discussion shows that the timing observations place quite stringent constraints on the physical picture, as summarized in Table 2. Some specific scenarios for jet formation, in which the jets and tori occur in the wrong sequence, or are unconnected, or have time scales that are too long, are ruled out or made implausible. The relatively sudden ejection of a discrete torus followed by jets on a short time scale most naturally fits the types of scenario in which a companion directly interacts with the central star. The physical situations in these scenarios are quite different, but theoretical exploration has not yet gone much beyond order of magnitude estimates. More realistic simulations are needed to predict the detailed characteristics of specific models so that we can discriminate among the possibilities.

5. Conclusions

The objects described in this paper cover a range in evolution from AGB stars to young PNe, but they all exhibit high velocity polar jets and dense equatorial molecular tori. From analysis of the timing of the jets and tori we reach the following conclusions.

First, the launching of the jets is approximately simultaneous with the ejection of the

tori. This implies a close connection between the two, and provides important information on the physical system in which the jets are formed.

Second, there is evidence for a torus-jet sequence. In some cases the observations are consistent with close or exact simultaneity, but the ensemble of data suggest a torus-jet sequence with a median jet-lag ~ 300 yr. The main uncertainty here is the possible role of jet acceleration. This has a somewhat similar effect as a delay, but is probably not the dominant effect.

Third, the ejection velocities and time scales provide further constraints on the physical picture. The low expansion velocities of the tori in particular may pose a challenge for models in which tori are ejected from the deep potential well of a common envelope.

These findings already rule out or make implausible several jet formation scenarios. Overall, the relatively sudden ejection of a discrete torus followed by jets on a short time scale most naturally fits the types of scenario in which a companion interacts with the central star. More detailed simulations of specific models are needed to help us discriminate among the possibilities.

It is a pleasure to acknowledge collaborative programs with R. Bachiller, P. Cox, and T. Forveille, the results of which form the basis of this paper. I thank E. Blackman, T. Forveille, and A. Frank for comments on the manuscript. This work has been supported in part by NSF grant AST 03-07277.

A. Details of the Observations

This appendix provides further information on the origin and determination of the quantities given in Table 1, and shown in Figs. 1 and 2.

A.1. Inclination Angles

The inclinations of the jets and tori to the line of sight (θ_j and θ_t) are important for estimating the expansion time scales because of projection effects. For the jets, the observed radial extents and velocities are $r_j \sin \theta_j$ and $v_j \cos \theta_j$, respectively, where r_j and v_j are the actual (un-projected) values. For the tori, the radii r_t are seen directly on the sky at the systemic velocity, and the maximum observed radial velocities are $v_t \sin \theta_t$. The expansion time scales, t_j and t_t , are therefore sensitive to the inclination angle, and vary as $\cot \theta_j$

and $\sin \theta_t$, respectively. Exceptions for which the expansion time scales are determined in a different way are noted below.

The adopted inclination angles for each source are given in Table 3, together with estimates of the uncertainty. In five sources there are independent estimates of θ_t and θ_j , and in the others there are estimates of only one: for these we assume that $\theta_t = \theta_j$. This is reasonable on the basis of the similarity where there are independent estimates, and by the fact that many (though not all) images show that jets are roughly aligned with the axes of the tori when seen in projection.

The uncertainties adopted for the inclination angles given in Table 2 are of two types. In specific cases noted in the footnotes to the table, the values of $\Delta\theta$ are taken from the references cited. For the others we have made rough estimates, based on the the observations and, where relevant, on the agreement between different estimates: for simplicity in these cases we have adopted values for $\Delta\theta$ of $\pm 5^\circ$ or $\pm 10^\circ$. For the sources where we assume $\theta_t = \theta_j$, the errors in Fig. 1 are correlated; and for the three objects in which t_j is estimated directly from proper motions, the results are independent of the inclination.

A.2. Notes on Individual Sources

KjPn 8.– θ_t is re-determined from the velocity strip maps of the torus (Forveille et al. 1998), and agrees with θ_j from the jet kinematics given by Meaburn (1997). t_j is from optical proper motions of the jets, $34 \pm 3 \text{ mas yr}^{-1}$ (Meaburn 1997).

M 1-16.– The adopted value of θ_j (from Schwarz 1992) is at the top of the range given by Corradi & Schwarz (1993); this value is preferred because the jets align with the torus axis on the sky and this is the closest value to θ_t , which is well determined. The inner edge of molecular torus is not well resolved by the CO observations; the limit in Fig. 2 corresponds to the radius of the small ionized nebula. t_j for the two additional jet components in Fig. 2 are 1050 yr and 740 yr (Schwarz 1992).

M 2-9.– t_j is from optical proper motions of the jets, $51 \pm 7 \text{ mas yr}^{-1}$ (Schwarz et al. 1997).

M 1-92.– The adopted value of $\theta_j = 57 \pm 5^\circ$ (Solf 1994) is from a geometrical method using Doppler shifts in the jets. t_t and t_j are based on the equatorial and polar velocity gradients (12 and $7.6 \text{ km s}^{-1} \text{ arcsec}^{-1}$, respectively) given by Alcolea et al. (2007); using the gradient for the torus gives a value of t_t that depends on $\tan \theta_t$. The gradient suggests a torus ejection event, although the jet outflows in this source are particularly wide-angle

and extend to low latitudes so that the torus may be wind-swept; this may account for the gradient. Alcolea et al. (2007) assume the torus and jets are ejected at the same time, which requires an inclination angle of 51.5° to get the same expansion time scales. In Figs. 1 and 2 we use the independent value of Solf (1994) given above.

M 2-56.– The inner rim of torus not well resolved; the limit in Fig. 2 corresponds to half the beamsize.

He 3-1475.– The data for the torus are uncertain because it is marginally resolved by the CO observations. The adopted values are from the CO model by Huggins et al. (2004). Other rough estimates give comparable values for t_t . For example, the strong, low velocity OH masers are spread over an area of radius $\sim 0''.5$ and a velocity of $\sim 18 \text{ km s}^{-1}$ (Zijlstra et al. 2001); this gives $t_t \sim 1000 \text{ yr}$. t_j is from optical proper motions of the jets, $12.6 \pm 1.1 \text{ mas yr}^{-1}$ (Riera et al. 2003). The younger jets shown in Fig. 2 have $t_j = 446 \text{ yr}$, from proper motions for knots NW2 and SW2 given by Riera et al. (2003).

V Hya.– r_t is the half power radius at the systemic velocity in the CO 3–2 line from the maps by Hirano et al. (2004). The inner rim is not well resolved, the limit in Fig. 2 corresponds to half the beamsize.

AFGL 618.– The data for the torus are uncertain because it is marginally resolved by the CO observations. The adopted values are from the CO model by Sánchez Contreras et al. (2004) with velocity \propto radius; the inner rim is not resolved. Roughly the same value of t_t ($\sim 400 \text{ yr}$) is obtained independently from an expanding torus model of the dense inner regions ($r_t \sim 0''.75$, $v_t \sim 5\text{--}12 \text{ km s}^{-1}$) observed in HC₃N (Pardo et al. 2004). θ_j is for the single jet b in the nomenclature of Trammell & Goodrich (2002) and v_j is the H₂ velocity for same jet (Cox et al. 2003).

π^1 Gru.– Data for the torus are from the CO model by Chiu et al. (2006); r_t is the geometric mean of the inner and outer model radii.

REFERENCES

- Alcolea, J., Bujarrabal, V., Sánchez Contreras, C., Neri, R., & Zweigle, J. 2001, *A&A*, 373, 932
- Alcolea, J., Neri, R., & Bujarrabal, V. 2007, *A&A*, in press, astro-ph/0701455
- Balick, B., & Frank, A. 2002, *ARA&A*, 40, 439
- Barnbaum, C., Morris, M., & Kahane, C. 1995, *ApJ*, 450, 862

- Bell, K. R., & Lin, D. N. C. 1994, *ApJ*, 427, 987
- Borkowski, K. J., & Harrington, J. P. 2001, *ApJ*, 550, 778
- Bujarrabal, V., Alcolea, J., & Neri, R. 1998, *ApJ*, 504, 915
- Castro-Carrizo, A., Bujarrabal, V., Sánchez Contreras, C., Alcolea, J., & Neri, R. 2002, *A&A*, 386, 633
- Chiu, P.-J., Hoang, C.-T., Dinh-V-Trung, Lim, J., Kwok, S., Hirano, N., & Muthu, C. 2006, *ApJ*, 645, 605
- Corradi, R. L. M., & Schwarz, H. E. 1993, *A&A*, 278, 247
- Corradi, R. L. M. 2004, *ASP Conf. Ser. 313: Asymmetrical Planetary Nebulae III: Winds, Structure and the Thunderbird*, 313, 148
- Corradi, R. L. M. 2004, *ASP Conf. Ser. 313: Asymmetrical Planetary Nebulae III: Winds, Structure and the Thunderbird*, 313, 558
- Cox, P., Lucas, R., Huggins, P. J., Forveille, T., Bachiller, R., Guilloteau, S., Maillard, J. P., & Omont, A. 2000, *A&A*, 353, L25
- Cox, P., Huggins, P. J., Maillard, J.-P., Muthu, C., Bachiller, R., & Forveille, T. 2003, *ApJ*, 586, L87
- Forveille, T., Huggins, P. J., Bachiller, R., & Cox, P. 1998, *ApJ*, 495, L111
- Frank, A., & Blackman, E. G. 2004, *ApJ*, 614, 737
- García-Arredondo, F., & Frank, A. 2004, *ApJ*, 600, 992
- García-Segura, G., López, J. A., & Franco, J. 2005, *ApJ*, 618, 919
- Hirano, N., et al. 2004, *ApJ*, 616, L43
- Huggins, P. J., Forveille, T., Bachiller, R., & Cox, P. 2000, *ApJ*, 544, 889
- Huggins, P. J., Muthu, C., Bachiller, R., Forveille, & Cox, P. 2004, *A&A*, 414, 581
- Huggins, P. J., & Manley, S. P. 2005, *PASP*, 117, 665
- Iben, I. J., & Livio, M. 1993, *PASP*, 105, 1373
- Imai, H., Obara, K., Diamond, P. J., Omodaka, T., & Sasao, T. 2002, *Nature*, 417, 829

- Knapp, G. R., Dobrovolsky, S. I., Ivezić, Z., Young, K., Crosas, M., Mattei, J. A., & Rupen, M. P. 1999, *A&A*, 351, 97
- Lee, C.-F., Stone, J. M., Ostriker, E. C., & Mundy, L. G. 2001, *ApJ*, 557, 429
- Lee, C.-F., & Sahai, R. 2003, *ApJ*, 586, 319
- Mastrodemos, N., & Morris, M. 1999, *ApJ*, 523, 357
- Matt, S., Frank, A., & Blackman, E. G. 2006, *ApJ*, 647, L45
- Mauron, N., & Huggins, P. J. 2006, *A&A*, 452, 257
- Meaburn, J. 1997, *MNRAS*, 292, L11
- Meixner, M., Kastner, J. H., Balick, B., & Soker, N. 2004, *ASP Conf. Ser.* 313: Asymmetrical Planetary Nebulae III: Winds, Structure and the Thunderbird
- Mitchell, D. L., Pollacco, D., O'Brien, T. J., Bryce, M., López, J. A., Meaburn, J., & Vaytet, N. M. H. 2006, *MNRAS*, 1422
- Morris, M. 1987, *PASP*, 99, 1115
- Nordhaus, J., & Blackman, E. G. 2006, *MNRAS*, 370, 2004
- Olofsson, H. 2003, in *Asymptotic giant branch stars*, ed. H. J. Habing & H. Olofsson. (Berlin: Springer), 325
- Pardo, J. R., Cernicharo, J., Goicoechea, J. R., & Phillips, T. G. 2004, *ApJ*, 615, 495
- Pastetter, L., & Ritter, H. 1989, *A&A*, 214, 186
- Reyes-Ruiz, M., & López, J. A. 1999, *ApJ*, 524, 952
- Riera, A., García-Lario, P., Manchado, A., Bobrowsky, M., & Estalella, R. 2003, *A&A*, 401, 1039
- Sabin, L., Zijlstra, A. A., & Greaves, J. S. 2007, *MNRAS*, in press
- Sahai, R., & Trauger, J. T. 1998, *AJ*, 116, 1357
- Sánchez Contreras, C., Bujarrabal, V., Castro-Carrizo, A., Alcolea, J., & Sargent, A. 2004, *ApJ*, 617, 1142
- Sandquist, E. L., Taam, R. E., Chen, X., Bodenheimer, P., & Burkert, A. 1998, *ApJ*, 500, 909

- Schwarz, H. E. 1992, *A&A*, 264, L1
- Schwarz, H. E., Aspin, C., Corradi, R. L. M., & Reipurth, B. 1997, *A&A*, 319, 267
- Shakura, N. I., & Sunyaev, R. A. 1973, *A&A*, 24, 337
- Soker, N., & Livio, M. 1994, *ApJ*, 421, 219
- Soker, N. 1996, *ApJ*, 468, 774
- Soker, N., & Rappaport, S. 2000, *ApJ*, 538, 241
- Solf, J. 1994, *A&A*, 282, 567
- Theuns, T., & Jorissen, A. 1993, *MNRAS*, 265, 946
- Trammell, S. R., & Goodrich, R. W. 2002, *ApJ*, 579, 688
- Ueta, T., Murakawa, K., & Meixner, M. 2006, *ApJ*, 641, 1113
- Zijlstra, A. A., Chapman, J. M., te Lintel Hekkert, P., Likkell, L., Comeron, F., Norris, R. P., Molster, F. J., & Cohen, R. J. 2001, *MNRAS*, 322, 280
- Zweigle, J., Neri, R., Bachiller, R., Bujarrabal, V., & Grewing, M. 1997, *A&A*, 324, 624

Table 1. Properties of the Jets and Tori

Name	d (kpc)	r_t (10^{16} cm)	v_t (km s^{-1})	t_t (yr)	r_j (10^{17} cm)	v_j (km s^{-1})	t_j (yr)	Δt (yr)	$\Delta t/t_t$	ref
KjPn 8	1.60	9.3	5.9	5040	34.6	314	3380 ^a	1660	0.33	1, 2
M 1-16	1.80	6.2	9.8	2000	17.8	350	1610 ^b	390	0.20	3, 4
M 2-9	0.64	2.9	7.0	1300	5.93	164	1170 ^a	130	0.10	5, 6
M 1-92	2.50	2.6	5.5	1520	2.21	69	1010 ^c	510	0.34	7, 8
M 2-56	2.10	4.4	8.0	1750	4.27	128	1060 ^c	690	0.39	9
He 3-1475	5.80	3.9	14	878	10.4	527	611 ^a	267	0.30	10, 11
V Hya	0.38	2.7	16	543	1.29	161	254 ^c	289	0.53	12
AFGL 618	0.90	1.6	12	422	0.97	222	139 ^c	283	0.67	13, 14, 15
π^1 Gru	0.15	1.2	11	354	0.09	55	54 ^c	300	0.85	16

^abased on optical proper motions

^bbased on optical kinematics

^cbased on molecular line kinematics

References. — (1) Forveille et al. 1998; (2) Meaburn 1997; (3) Huggins et al. 2000; (4) Schwarz 1992; (5) Zweigle et al. 1997; (6) Schwarz et al. 1997; (7) Bujarrabal et al. 1998; (8) Alcolea et al. 2007; (9) Castro-Carrizo et al. 2002; (10) Huggins et al. 2004; (11) Riera et al. 2003; (12) Hirano et al. 2004; (13) Cox et al. 2003; (14) Trammell & Goodrich 2002; (15) Sánchez Contreras et al. 2004; (16) Chiu et al. 2006

Table 2. Jet-Torus Scenarios

Scenario	Rating	Comments
Magnetic wind from single star	–	jets <i>and</i> torus?
Primary mass loss + companion accretion disk	★	discrete torus ejection?
Companion accretion disk + CE ejection	–	wrong sequence
CE ejection + magnetic polar wind	★	jet-lag?
(CE) magnetic polar & equatorial explosion	★	jet-lag?
(CE) primary accretion disk + late nebula ejection	–	wrong sequence
CE partial ejection + primary accretion disk	★	jet-lag?
CE ejection + post-CE primary accretion disk (RLOF)	–	time scale too long?

Note. — CE = Common Envelope, RLOF = Roche lobe overflow

Table 3. Inclination Angles

Name	θ_t ($^\circ$)	θ_j ($^\circ$)	$\pm\Delta\theta$ ($^\circ$)	ref
KjPn 8	52	53	5	1, 2
M 1-16	54	45	10	3, 4
M 2-9	73	75	5	5, 6
M 1-92	57 ^a	57	5 ^b	7
M 2-56	73	73 ^a	2 ^b	8
He 3-1475	40	40	5	9, 10
V Hya	30	30 ^a	10	11
AFGL 618	58	51	10, 4 ^b	12, 13
π^1 Gru	35	35 ^a	10	14

^aAssuming $\theta_j = \theta_t$

^bEstimate from reference, others from this paper.

References. — (1) Forveille et al. 1998; (2) Meaburn 1997; (3) Huggins et al. 2000; (4) Schwarz 1992; (5) Zweigle et al. 1997; (6) Schwarz et al. 1997; (7) Solf 1994; (8) Castro-Carrizo et al. 2002; (9) Borkowski & Harrington 2001; (10) Huggins et al. 2004; (11) Hirano et al. 2004; (12) Sánchez Contreras et al. 2004; (13) Trammell & Goodrich 2002; (14) Chiu et al. 2006

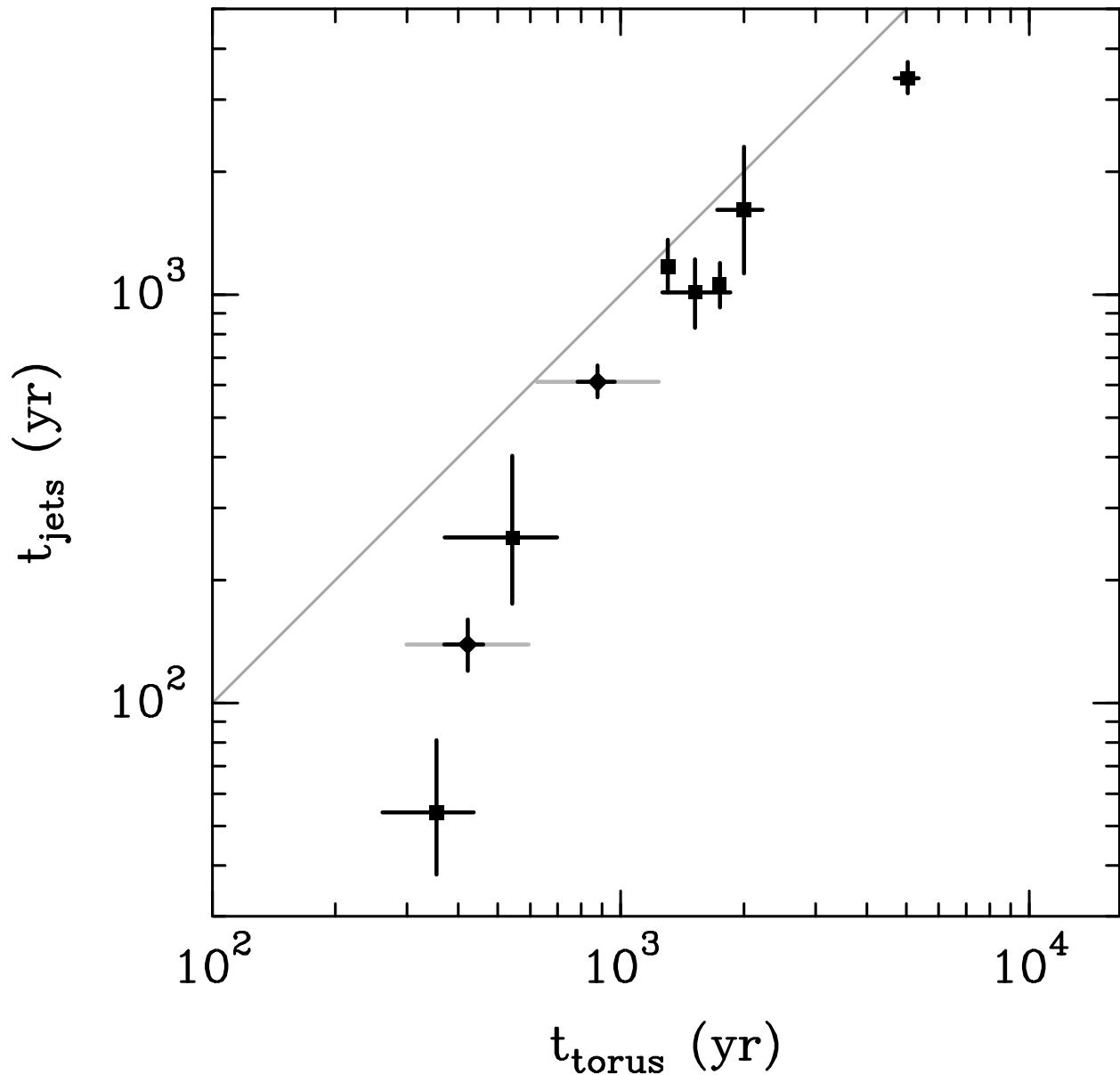


Fig. 1.— Comparison of the expansion times of the jets and tori. The squares denote cases where the tori are resolved, and the diamonds where they are marginally resolved. The error bars reflect the uncertainties in the inclination angles or proper motions. The extra, gray error bars reflect a nominal factor of 2 uncertainty in the dimensions of the marginally resolved tori. The continuous line shows the locus on which the expansion time scales are equal.

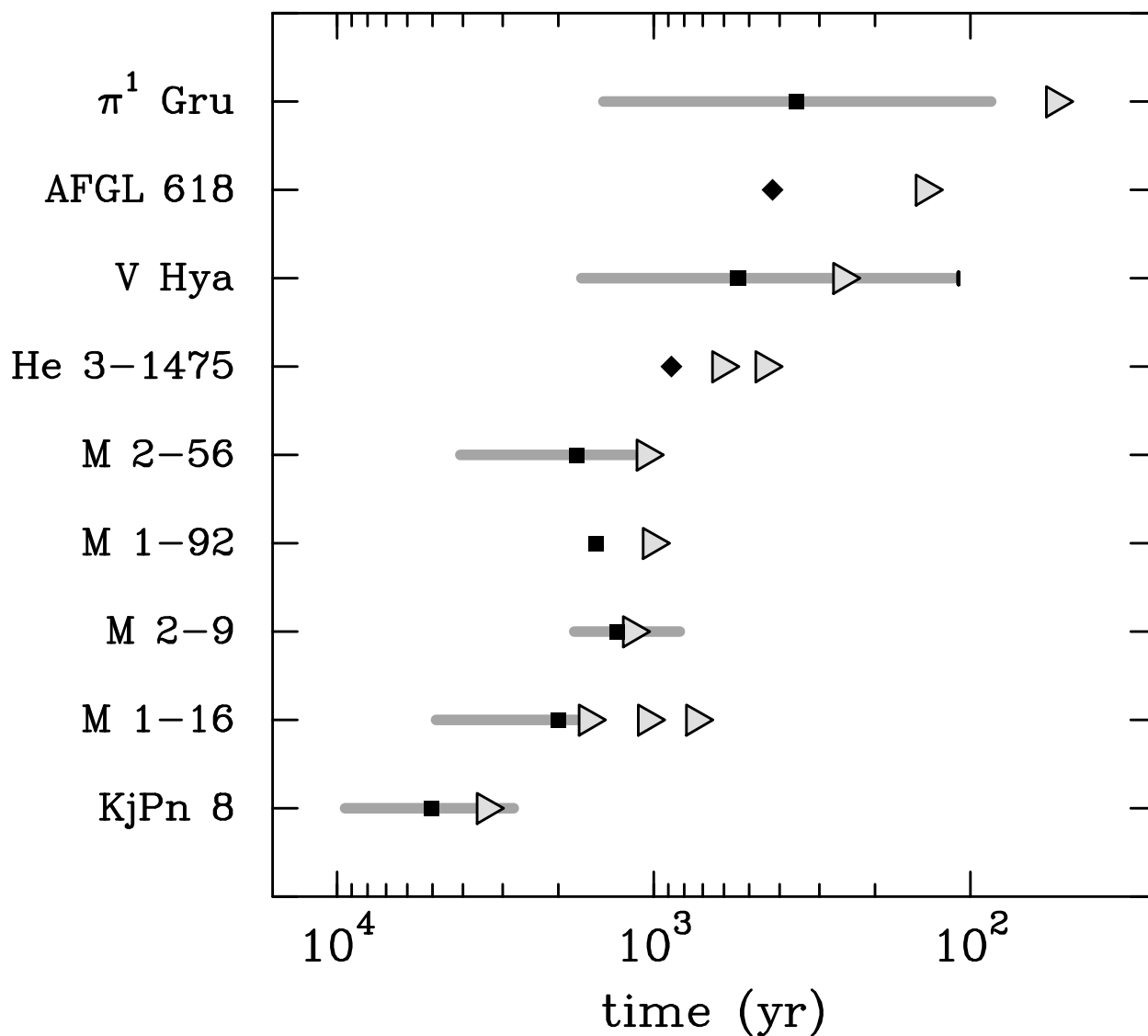


Fig. 2.— Time sequence for the ejection of jets and tori. The horizontal axis is time in the past, measured from the current epoch. The filled squares and diamonds show the fiducial times of torus ejection as in Fig. 1. The horizontal lines show the characteristic duration of the torus ejection, assuming a constant ejection velocity. In cases where the inner rim of the torus is not seen, the time line is truncated with a small vertical line corresponding to the resolution limit. Data for the time lines of the marginally resolved cases (diamonds) are incomplete. M 1-92 may be ejected in a single event. The triangles denote the times of jet ejection. Data on the multiple jets in He 3-1475 and M 1-16 are given in the appendix.